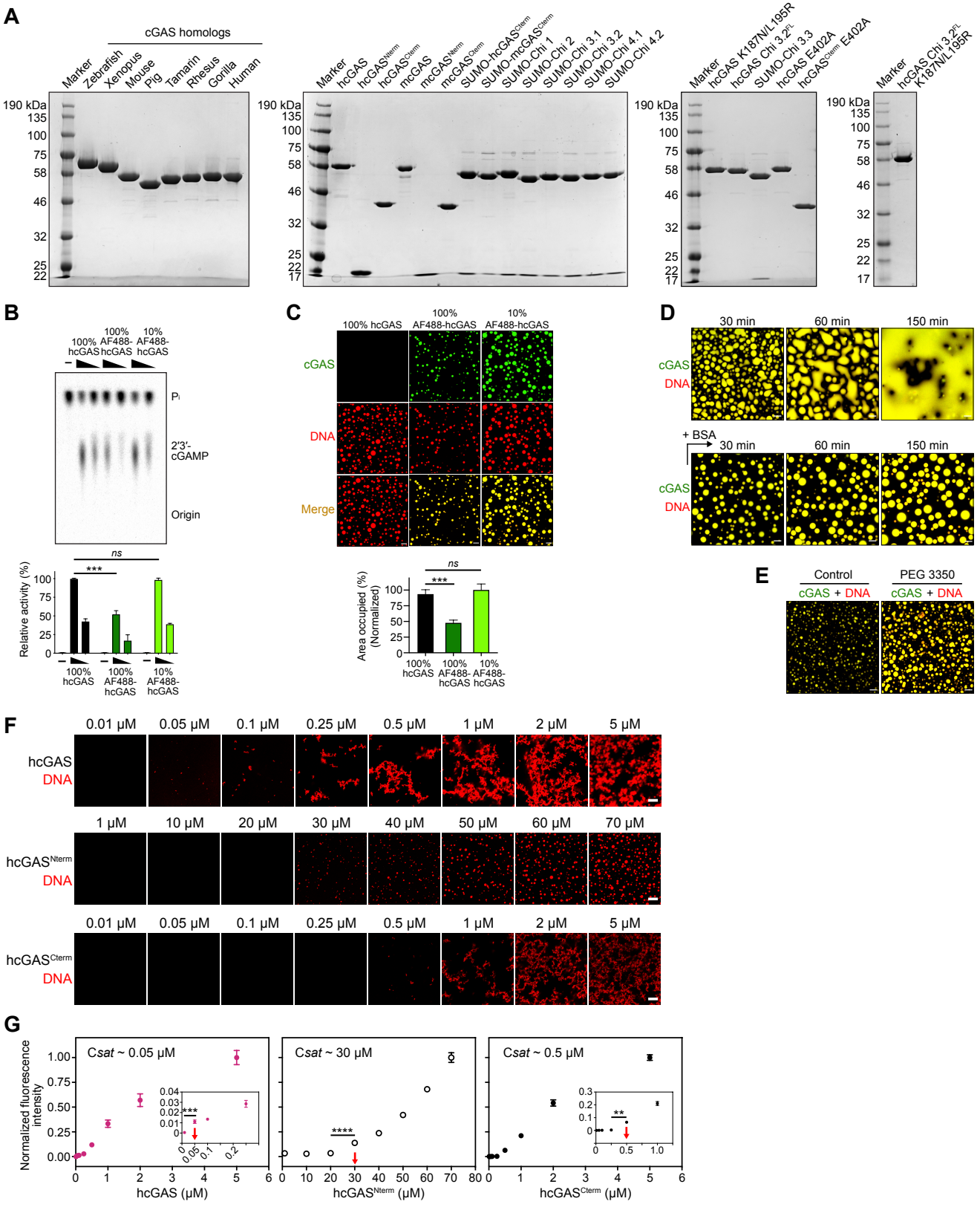

Figure S1. The properties of human cGAS-DNA phase separation, related to Figure 1

(A) SDS-PAGE and Coomassie analysis of purified cGAS proteins (~1 μg) used in this study. 6×His-SUMO2-tagged cGAS chimeras (denoted SUMO-) were purified with Ni-NTA affinity and were used for mapping the

molecular determinant of enhanced phase separation of hcGAS. All other experiments were performed with untagged proteins purified with Ni-NTA affinity, heparin ion-exchange, and size-exclusion chromatography. FL, full length.

(B,C) Analysis of the impact of cGAS labeling on 2′3′-cGAMP synthesis activity and phase separation. B, 2′3′-cGAMP synthesis with unlabeled hcGAS and AF488-labeled hcGAS assessed and quantified by thin-layer chromatography and phosphorimaging (see STAR Methods). C, fluorescence microscopy images of cGAS-DNA droplets using different ratios of labeled- and unlabeled cGAS. AF488-labeled hcGAS exhibits reduced 2′3′-cGAMP production and weaker phase separation compared to unlabeled hcGAS, likely due to the disruption of positively-charged amino acids in cGAS. However, the mixture of unlabeled hcGAS with 10% AF488-labeled hcGAS does not impact hcGAS function including both enzymatic activity and phase separation. Therefore, a 10% AF488-labeled hcGAS mixture was used to observe cGAS in all fluorescence microscopy experiments in this study unless otherwise indicated. Scale bar, 10 μm. All data are expressed as the mean ± SEM of 3 independent experiments (B) and 5 images in 3 independent experiments (C). Statistical significance was calculated with a two-tailed T test, ***p = <0.001, ns >0.1.

(D) Time-lapse fluorescence microscopy images showing wetting property of cGAS-DNA droplets on the coverslip surface. In the presence of 1 mg mL^{-1} BSA, cGAS-DNA droplets maintain spherical property over time. Therefore, BSA (final concentration at 1 mg mL^{-1}) was used to suppress droplet wetting in all fluorescence microscopy experiments in this study unless otherwise indicated. Scale bar, 10 μm.

(E) Fluorescence microscopy images showing the macro-molecular crowding agent PEG-3350 enhances cGAS-DNA phase separation. hcGAS (5 μM, containing 1 μM AF488-labeled cGAS) was incubated with 100 bp dsDNA (5 μM, containing 1 μM Cy3-labeled DNA) at 250 mM salt (total NaCl and KCl) with or without 5% PEG -3350. Scale bar, 10 μm.

(F) Fluorescence microscopy images of hcGAS protein phase separation at varying protein and DNA concentrations. Phase separation was induced using equal amounts of protein and DNA at a range of concentrations as indicated with a constant salt (total NaCl and KCl) concentration of 150 mM. Scale bar, 10 μm.

(G) Fluorescence intensity analysis and quantification of microscopy images in (F). All data are expressed as the mean ± SEM of 6 images in 3 independent experiments. Statistical significance was calculated with a two-tailed T test, ****p = <0.0001, ***p = <0.001, **p = <0.01.

Scale bar, 10 μm.

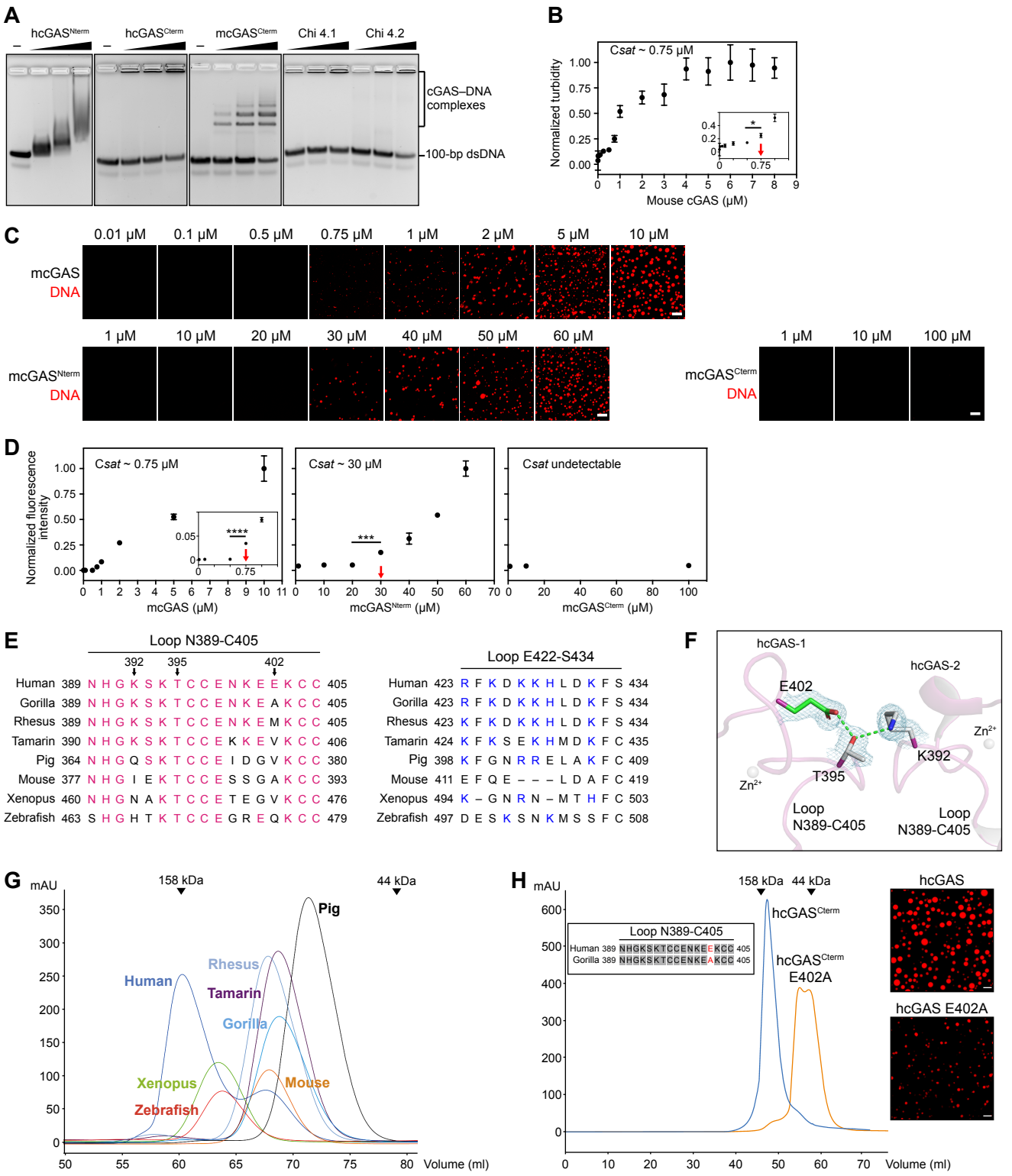

Figure S2. Enhanced phase separation of human cGAS is controlled via additional cGAS-cGAS and cGAS-DNA interactions, related to Figure 1

(A) *In vitro* electrophoretic mobility shift assay measurement of cGAS–DNA complex formation. cGAS N- and C-terminal chimeras (0.5, 1, 2 μM) were incubated with 100 bp dsDNA (1 μM) in the presence of 75 mM KCl, and the resulting complexes were resolved on a 2% agarose gel. Data are representative of two independent experiments.

(B) Turbidity assay analysis of the relative saturation concentrations of mcGAS. A series of concentrations of mcGAS with DNA (equal ratio) were mixed at 150 mM salt, and turbidity was measured according to absorbance at 340 nm. The relative saturation concentrations were determined by a two-tailed T test of the adjacent values across each pair of points in the protein/DNA titration and are indicated with red arrows. Data were normalized to the maximal value as 1.00. Data are the mean ± SEM of 4 independent experiments. Statistical significance was calculated with a two-tailed T test, *p = <0.1.
(C) Fluorescence microscopy images of mouse cGAS (mcGAS) phase separation at varying protein and DNA concentrations. Phase separation was induced as in Figure S1F. Scale bar, 10 μm.
(D) Fluorescence intensity analysis and quantification of microscopy images in (C). Data are the mean ± SEM of at least 6 images in 3 independent experiments. Statistical significance was calculated with a two-tailed T test, ****p = <0.0001, ***p = <0.001.
(E) Sequence alignment of cGAS loops N389–C405 and E422–S434 within vertebrate species. The amino acid residues that are identical to human cGAS in loop N389–C405 are highlighted in magenta. The residues of E402, T395, and K392 highlighted in (F) are marked with arrows. Positively charged residues in loop E422–S434 are denoted in blue.
(F) Overview of the locations of E402, T395, and K392 in the apo hcGAS structure (PDB: 4LEV) with $2F_O–F_C$ electron density map contoured at 1.0 σ.
(G) Size-exclusion chromatography analysis of cGAS homologs compared to molecular weight protein standards suggests at high protein concentrations human cGAS has a propensity to adopt a dimer-like conformation even in the absence of DNA.
(H) Left, size-exclusion chromatography analysis of hcGAS E402A suggests that this substitution in the hcGAS loop N389–C405 specifically reduces protein-protein interactions in the hcGAS dimeric complex. Right, fluorescence microscopy images of hcGAS phase separation analysis demonstrates the E402A substitution inhibits liquid droplet formation. Scale bar, 10 μm.

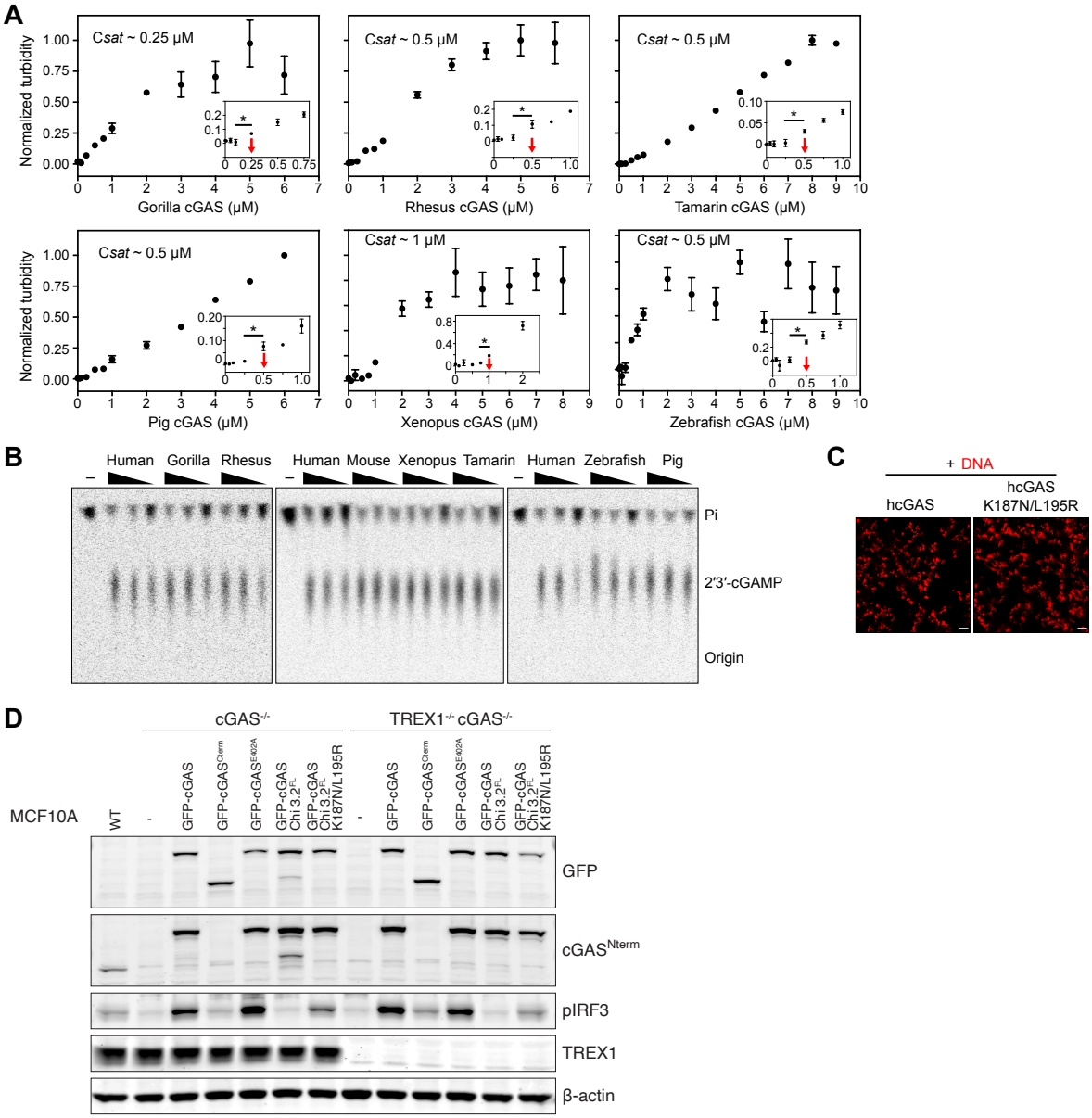

Figure S3. cGAS phase separation does not directly control 2′3′-cGAMP synthesis *in vitro* but is required for immune activation in cells, related to Figure 2

(A) Turbidity assay analysis of the relative saturation concentrations of cGAS homologs. The relative saturation concentrations (red arrows) of 6 cGAS homologs were determined by turbidity assay as in Figure S2B. Data are the mean ± SEM of at least 4 independent experiments. Statistical significance was calculated with a two-tailed T test, *p = <0.1.

(B) *In vitro* analysis of the ability of vertebrate cGAS homologs to synthesize 2′3′-cGAMP. cGAS proteins (3.0, 1.0, 0.33 μM) were incubated with 100 bp dsDNA (1 μM) at 60 mM KCl, and relative 2′3′-cGAMP synthesis was determined by thin-layer chromatography as in Figure S1B. The relative 2′3′-cGAMP synthesis of cGAS proteins at 3 μM was used for the quantification in Figure 2D. Data are representative of three independent experiments.

(C) A previously mapped hcGAS K187N/L195R substitution that enhances 2′3′-cGAMP synthesis does not impact cGAS-DNA phase separation. hcGAS variants (10 μM each) were incubated with 100 bp dsDNA (10 μM, containing 1 μM Cy3-labeled DNA) at 150 mM salt (total NaCl and KCl).

(D) Immunoblot analysis of cGAS expression, TREX1 expression, and accumulation of phosphorylated IRF3 (pIRF3) upon stimulation with plasmid DNA in cGAS$^{-/-}$ or cGAS$^{-/-}$ TREX1$^{-/-}$ MCF10A cells as indicated.

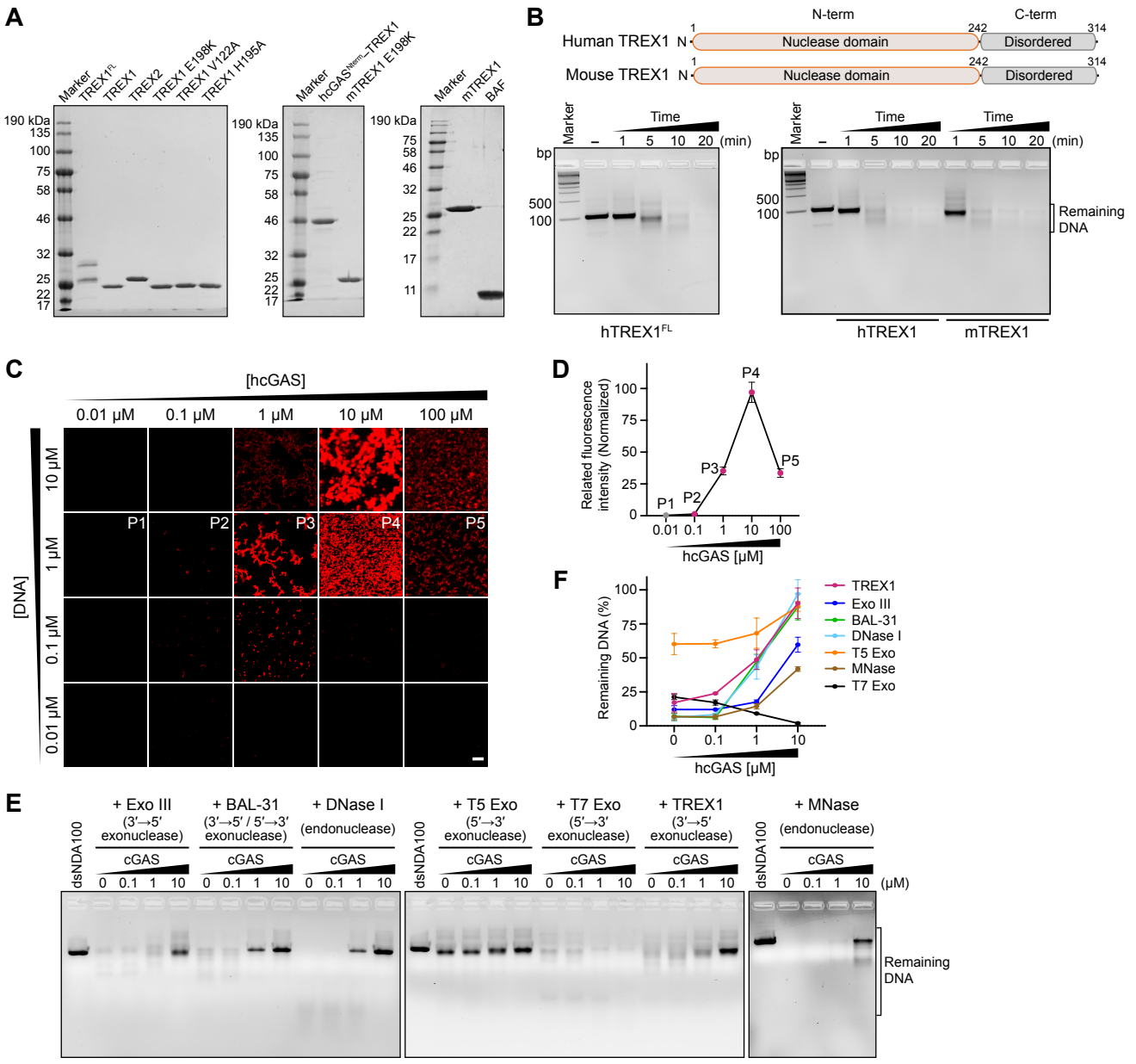

Figure S4. cGAS-DNA phase separation resists DNA degradation by the exonuclease TREX1, related to Figure 3

(A) SDS-PAGE and Coomassie analysis of purified TREX1 proteins and BAF (~1 μg) used in this study. All TREX1 proteins were purified with Ni-NTA affinity, heparin ion-exchange, and size-exclusion chromatography. BAF was refolded and purified with Ni-NTA affinity and heparin ion-exchange (see STAR Methods).

(B) *In vitro* analysis of DNA degradation by human and mouse TREX1. Top, schematic of human and mouse TREX1. Bottom, DNase activity of full-length (denoted TREX1^{FL}) and nuclease domain-only human and mouse TREX1 (denoted hTREX1 and mTREX1). Degradation reactions were performed using 1 μM 100-bp dsDNA and 0.1 μM TREX1 proteins at 150 mM salt and the resulting reactions were resolved on 4% agarose gel.

(C) Fluorescence microscopy images used to assemble the hcGAS 2D phase diagram (Figure 3B). cGAS and DNA concentrations were used as indicated. Scale bar, 10 μm. The microscopy images of the cGAS-DNA condensates at 1 μM DNA (Points P1–P5) were used for the quantification of area occupied in Figure 3B.

(D) Fluorescence intensity analysis and quantification of microscopy images in (C). Data are normalized to the maximal value as 100. Data are the mean ± SEM of at least 6 images in 2 independent experiments.

(E) *In vitro* analysis of the impact of cGAS-DNA phase separation on DNase activity of various nucleases. Phase

separation was induced by 100 bp dsDNA (1 μM) and cGAS (increasing concentration at 0.1, 1, and 10 μM) at 150 mM salt for 30 min, and nucleases were added to the preformed cGAS-DNA condensates. The remaining DNA was resolved on a 4% agarose gel. The reaction buffer contains 5 mM $MgCl_2$ for all nucleases except MNase was additionally supplemented with 5 mM $CaCl_2$. Exo III, Exonuclease III. BAL-31, Nuclease BAL-31. T5 Exo, T5 Exonuclease. T7 Exo, T7 Exonuclease. MNase, Micrococcal nuclease.
(F) Quantification of DNA degradation by various nucleases in the presence of cGAS phase separation as in (E). Data are plotted as the mean ± SEM of 3 independent experiments.

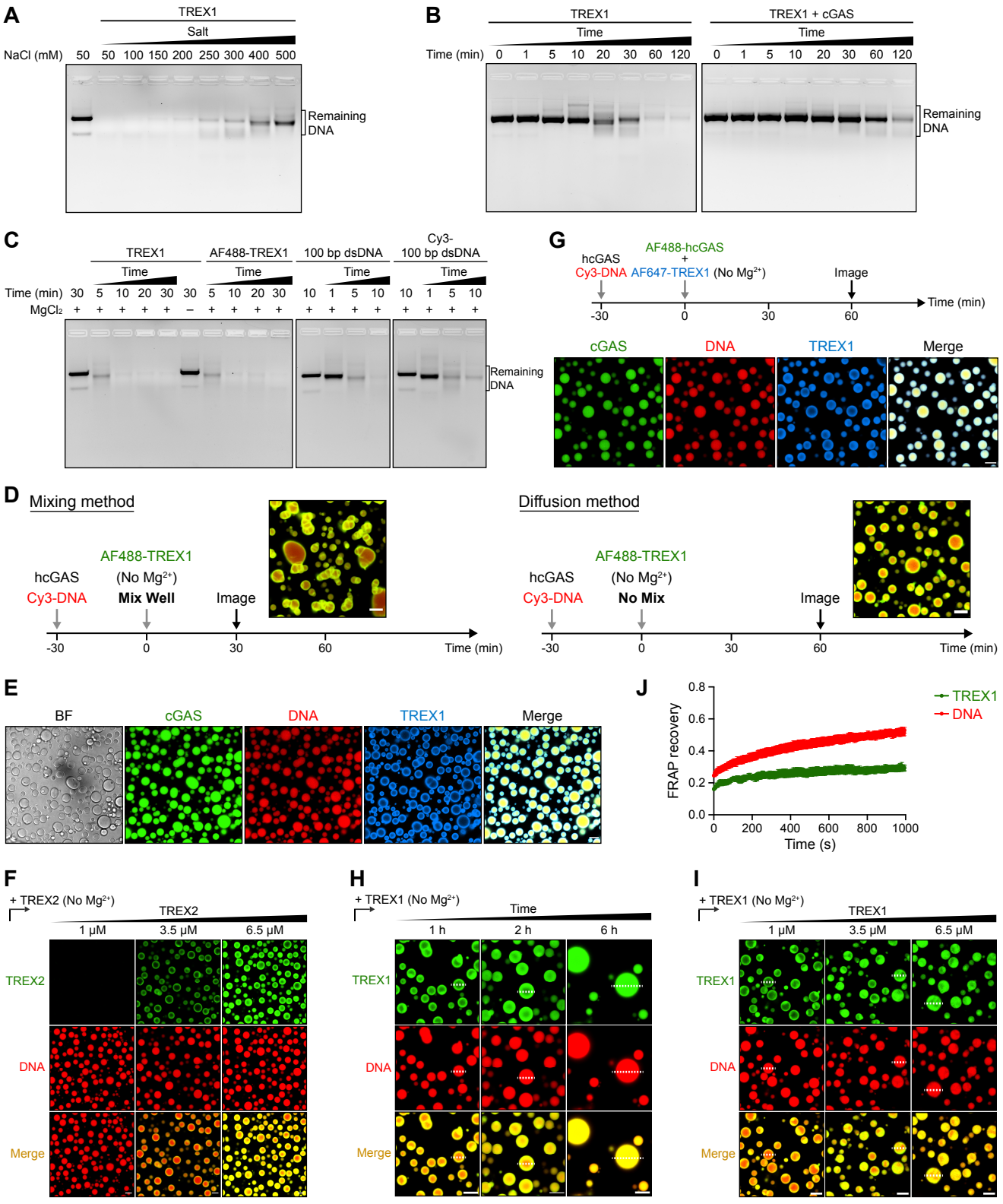

Figure S5. cGAS-DNA phase separation creates as selective environment that restricts TREX1 diffusion, related to Figures 4 and 5

(A) Analysis of impact of salt concentration on TREX1 dsDNA DNase activity. 0.1 μM hTREX1 was incubated with 1 μM 100 bp dsDNA at a gradient of salt concentrations as indicated (50–500 mM salt (total NaCl and KCl)) and the remaining DNA was visualized by agarose gel analysis.

(B) cGAS-DNA droplets protect DNA from TREX1 degradation. TREX1 DNA degradation was analyzed in the absence (left) or presence (right) of cGAS-DNA droplet formation. cGAS-DNA droplet formation was induced as in Figure 4B using unlabeled cGAS and DNA (10 μM each) at 250 mM salt. TREX1 DNA degradation was stimulated by adding Mg^{2+} to a final concentration of 5 mM and reactions were then incubated at 25°C for the indicated amount of time. The remaining DNA was resolved on 4% agarose gel.
(C) AF488- and Cy3-labeling do not significantly impact TREX1 exonuclease activity. Degradation reactions were conducted using ether AF488-labeled TREX1 or Cy3-labeled DNA, and subsequently the remaining DNA was resolved on 4% agarose gel. In the absence of Mg^{2+}, no detectable DNA degradation was observed confirming the strict metal-dependence of TREX1 activity (de Silva et al., 2007).
(D) Schematic of two methods to study the interactions between TREX1 and cGAS-DNA droplets. AF488-labeled TREX1 was added to preformed cGAS-DNA droplets, followed by ether directly mixing through pipetting up-and-down or allowing TREX1 to diffuse through the well of the imaging plate without mixing. For the Mixing method, a time of 30 min is required for the re-suspended droplets to settle to the bottom surface for imaging. However, 60 min is required to allow TREX1 to evenly distribute through the Diffusion method. To allow better visualization, the Diffusion method was used for all experiments unless otherwise indicated. Scale bar, 10 μm.
(E) Fluorescence microscopy images demonstrating a shell formation of TREX1 around cGAS-DNA droplets. cGAS-DNA-TREX1 droplet formation was induced as in Figure 4D without adding $MgCl_2$. The brightfield image is presented to the left. Scale bar, 10 μm.
(F) cGAS-DNA liquid droplets restrict localization of TREX2 to the outer droplet periphery. An increasing concentration of recombinant TREX2 was added to cGAS-DNA droplets as indicated. TREX2 exhibits the same phenotype as TREX1 demonstrating that cGAS-DNA droplets resist degradation of the human paralog of TREX1. Scale bar, 10 μm.
(G) Fluorescence microscopy images of AF488-cGAS (1 μM) and AF647-TREX1 (1 μM) simultaneously added to preformed cGAS-DNA droplets. Microscopy images were collected after 1 h incubation as indicated. Scale bar, 10 μm.
(H, I) cGAS-DNA phase separation limits diffusion of TREX1. Unlabeled hcGAS (10 μM) and 100-bp DNA (10 μM, containing 1 μM Cy3-labeled DNA) were used to induce droplet formation, followed by adding TREX1 (containing 1 μM AF488-labeled TREX1). Microscopy images were collected with (H) an increasing duration of time after TREX1 addition or (I) an increasing concentration of TREX1 as indicated. Dotted lines indicate the randomly selected droplets which are used for intensity calculation in Figure 5B. Scale bar, 10 μm.
(J) FRAP analysis of the fluidity of TREX1 and DNA in preformed TREX1-cGAS-DNA droplets. AF488-labeled TREX1 was added to cGAS-DNA droplets and incubated until TREX1 was fully portioned throughout the droplet. Time 0 indicates the time of photo bleaching. Plots are generated from 6 droplets and data represent the mean ± SEM.

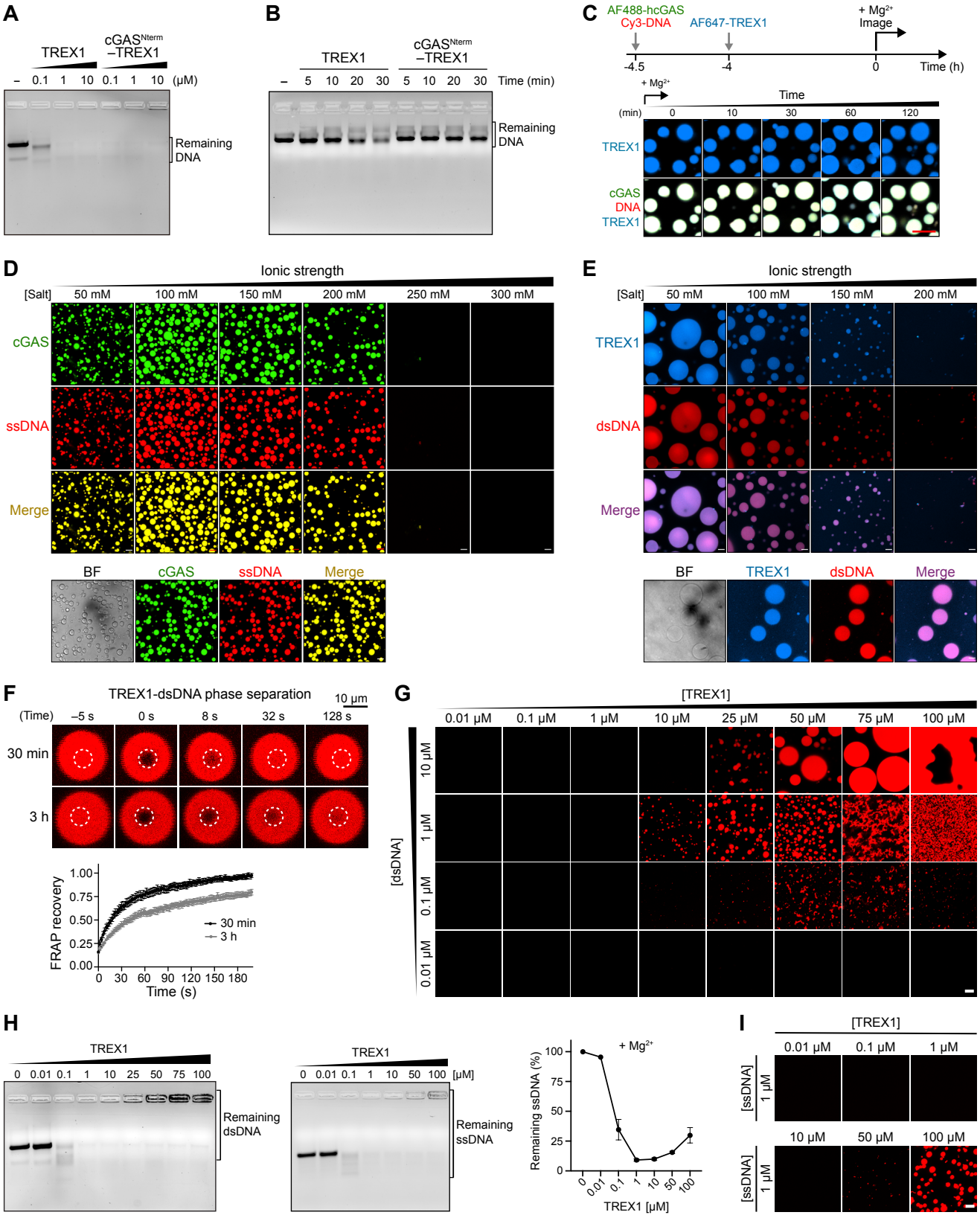

Figure S6. Phase separation is a direct repressor of TREX1 exonuclease activity, related to Figure 5

(A,B) *In vitro* activity assay of TREX1 and cGAS^{Nterm}–TREX1 with and without cGAS-DNA phase separation. An increasing concentration of TREX1 or cGAS^{Nterm}–TREX1 was incubated with 1 μM 100-bp dsDNA. The remaining

DNA was resolved on a 4% agarose gel.
(C) Time-lapse imaging of the inability of TREX1 to degrade DNA inside cGAS-DNA droplets. Droplet formation was induced by hcGAS (10 μM, containing 1 μM AF488-labeled hcGAS) and 100-bp DNA (10 μM, containing 1 μM Cy3-labeled DNA) for 30 min, and 1 μM AF647-labeled TREX1 was subsequently added to preformed cGAS-DNA droplets. Droplets were incubated for 4 h to ensure complete TREX1 incorporation (see Figure 5A) and 5 mM $MgCl_2$ was added to activate TREX1. Time 0 indicates the time of $MgCl_2$ addition. Scale bar, 10 μm.
(D) Fluorescence microscopy images of ssDNA-induced cGAS phase separation. hcGAS (10 μM, containing 1 μM AF488-labeled cGAS) was incubated with 100 bp ssDNA (10 μM, containing 1 μM Cy3-labeled ssDNA) for 30 min with increasing salt concentration as indicated. Bottom, brightfield and fluorescence microscopy images of hcGAS-ssDNA phase separation at 150 mM salt concentration. Scale bar, 10 μm.
(E) Fluorescence microscopy images of dsDNA-induced TREX1 phase separation. Phase separation was induced by 10 μM dsDNA (containing 1 μM Cy3-labeled dsDNA) and 20 μM TREX1 (containing 1 μM AF647-labeled dsDNA) for 30 min with increasing salt concentration as indicated. Bottom, brightfield and fluorescence microscopy images of TREX1-dsDNA phase separation at 100 mM salt concentration. Scale bar, 10 μm.
(F) FRAP analysis of TREX1-dsDNA droplets. TREX1-dsDNA droplet formation was induced as in (E) at 125 mM salt (total NaCl and KCl) for 30 min (top) or 3 h (bottom). Time 0 indicates the time of bleaching pulse. Plots are generated from 6 droplets and data represent the mean ± SEM.
(G) Fluorescence microscopy images used to assemble the TREX1-dsDNA 2D phase diagram in Figure 5I. hTREX1 and dsDNA concentrations were used as indicated. A reentrant phase transition may also occur for TREX1-DNA condensates (100 μM TREX1 to 0.1 μM DNA for example) but this phenomenon requires a TREX-1:DNA ratio of >1000× and is less readily observable than for hcGAS-DNA condensates (see Figure S4C). Scale bar, 10 μm.
(H) Analysis of ssDNA degradation by TREX1. TREX1-DNA complexes were assembled with 100 bp dsDNA (left gel image) or 100-bp ssDNA (right gel image) and increasing TREX1 concentration in the presence of 5 mM $MgCl_2$ and separated on an agarose gel for quantification. Prior to the agarose gel electrophoresis, reactions were treated at 75°C for 15 min. Without treatment of reactions with SDS and further DNA isolation by standard PCR clean-up (as in Figure 5J) the TREX1-DNA complexes typically remain in the gel well. Data represent the mean ± SEM of 4 independent experiments.
(I) Fluorescence microscopy images of TREX1-ssDNA assembly. hTREX1 and ssDNA concentrations were used as indicated. Scale bar, 10 μm.

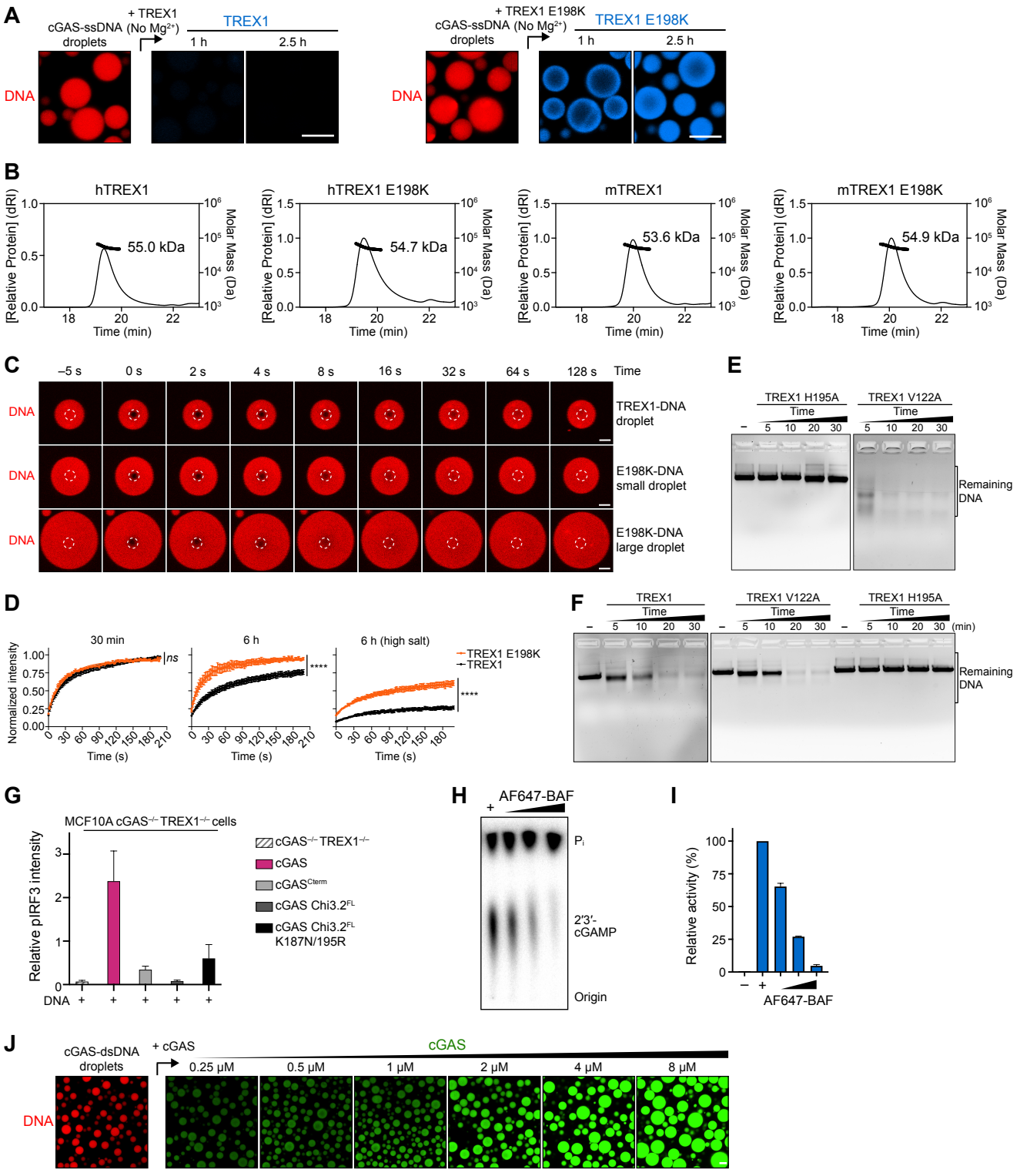

Figure S7. The disease mutation TREX1 E198K alters interactions with cGAS-DNA droplets, and cGAS phase separation resists immune suppression by negative regulators, related to Figure 7

(A) Time-lapse imaging of wildtype TREX1 and TREX1 E198K incubated with hcGAS-ssDNA droplets. Unlike wildtype TREX1, TREX1 E198K rapidly partitions into hcGAS droplets formed with ssDNA. cGAS-ssDNA droplets were formed by mixing cGAS and 100-nt ssDNA, and AF647-labeled TREX1 (left) or TREX1 E198K (right) were added to preformed cGAS-ssDNA droplets for analysis. Scale bar, 10 μm.

(B) Size-exclusion chromatography with multi-angle light scattering (SEC-MALS) analysis of hTREX1, hTREX1 E198K, mTREX1, and mTREX1 E198K.
(C) FRAP analysis of TREX1-dsDNA (top) and TREX1^{E198K}-dsDNA (middle and bottom) droplets formed with 100-bp dsDNA (10 μM, containing 1 μM Cy3-labeled DNA) and unlabeled TREX1 or TREX1 E198K protein for 3 h. TREX1 E198K typically forms larger droplets with DNA compared to wildtype TREX1. Both small and large droplets of TREX1 E198K exhibit increased recovery, demonstrating that enhanced fluidity of TREX1 E198K is not due to droplet size. Time 0 indicates the time of photobleaching pulse. Scale bar, 10 μm.
(D) Quantification of FRAP analysis demonstrates that TREX1^{E198K}-dsDNA droplets maintain fluidity longer than wildtype TREX1. TREX1-dsDNA and TREX1^{E198K}-dsDNA droplets were formed after incubation for 30 min at 125 mM salt (total NaCl and KCl), 6 h at 125 mM salt (total NaCl and KCl), or 6 h at 150 mM salt (total NaCl and KCl) (high salt). Time 0 indicates the time of photobleaching pulse. Plots are generated from 6 droplets and data represent the mean ± SEM. Statistical significance was calculated with a two-tailed T test, ****p = <0.0001, ns >0.1.
(E) *In vitro* analysis of exonuclease activity of TREX1 H195A and TREX1 V122A. Purified TREX1 mutants were incubated with 100-bp dsDNA at 150 mM salt (total NaCl and KCl) as indicated and remaining DNA was then resolved on 4% agarose gels. TREX1 H195A disrupts the enzyme active site and ablates all nuclease activity (Brucet et al., 2007). TREX1 V122A is a disease-associated mutation that does not impair exonuclease activity *in vitro* (Orebaugh et al., 2013).
(F) *In vitro* analysis of exonuclease activity of TREX1 and related mutants in the presence of hcGAS phase separation. hcGAS-DNA phase separation was induced by mixing hcGAS and DNA, and DNA degradation was initiated by adding TREX1 wildtype, TREX1 V122A, or TREX1 H195A for an increasing reaction time. The remaining DNA was resolved on 4% agarose gels.
(G) Quantification of immunoblot analysis of phosphorylated IRF3 (pIRF3) in MCF10A cGAS$^{-/-}$ TREX1$^{-/-}$ cells reconstituted with hcGAS, hcGAS^{Cterm} or hcGAS mutant alleles and transfected with plasmid DNA. Data are the mean ± SD of 3 experiments.
(H) Fluorescent labeling does not impact the ability of BAF to inhibit cGAS. AF647-labeled BAF was added to cGAS reactions as indicated and 2′3′-cGAMP synthesis was measured as in Figure S1B. Data are represented as mean ± SEM of 3 independent experiments.
(I) Quantification of AF647-labeled BAF-dependent cGAS inhibition experiments in (H). 2′3′-cGAMP synthesis was quantified as in Figure S1B. Data are represented as mean ± SEM of 3 independent experiments.
(J) Fluorescence microscopy images of dosage-dependent incorporation of cGAS into preformed cGAS-DNA droplets. cGAS-dsDNA droplet formation was induced as in Figure 5F with labeled DNA and non-labeled cGAS, and then AF488-labeled cGAS was added for incorporation analysis. Scale bar, 10 μm.